ADIABATIC DEMAGNETIZATION REFRIGERATOR FIELD MAPPING AND SHIELDING MODELS FOR A 70 MK SUPERCONDUCTING TRANSITION EDGE SENSOR ARRAY AND ASSOCIATED ELECTRONICS

D. R.Ladner[1], D. S. Martinez-Galarce[2], and D. McCammon[3]

[1]N-Science Corporation
Arvada, CO 80002, USA

[2]Lockheed Martin Solar and Astrophysics Laboratory
Palo Alto, CA 94304, USA

[3]University of Wisconsin
Madison, WI 53706, USA

ABSTRACT

An X-ray detection instrument to be flown on a sounding rocket experiment (the Advanced Technology Solar Spectroscopic Imager – ATSSI) for solar physics observations, is being developed by the Lockheed Martin Solar and Astrophysics Laboratory (LMSAL). The detector is a novel class of microcalorimeter, a superconducting Transition-Edge Sensor (TES), that coupled with associated SQUID and feedback electronics requires high temperature stability at ~100 mK to resolve the energy of absorbed X-ray photons emitted from the solar corona. The cooling system incorporates an existing Adiabatic Demagnetization Refrigerator (ADR) developed at the University of Wisconsin, which was previously flown to study the diffuse cosmic X-ray background. The Si thermistor detectors required 130 K shielded JFET electronic components that are much less sensitive to the unshielded external field of the ADR solenoid than are the 1st (~100mK) and 2nd (~2K) SQUID stages used with TESs. Modification of the Wisconsin ADR design, including TES focal plane and electronics re-positioning, therefore requires a tradeoff between the existing ADR solenoid corrector coil geometry and a low mass passive solenoid shield, while preserving the vibration isolation features of the existing design. We have developed models to accurately compute the magnetic field with and w/o shielding or corrector coils at critical locations to guide the re-design of the detector subsystem. The models and their application are described.

KEYWORDS: adiabatic demagnetization refrigerator (ADR), magnetic shielding, solenoid magnetic field model, solenoid shield model, transition edge sensor (TES), X-ray detector

PACS: 41.20.Gz, 07.55.Nk, 85.80.Jm, 84.71.Ba, 41.20.-q, 74.62.-c, 07.85.Fv

INTRODUCTION

Instrument Application

An X-ray detection instrument to be flown on a sounding rocket experiment (the Advanced Technology Solar Spectroscopic Imager – ATSSI) for solar physics observations, is being developed by the Lockheed Martin Solar and Astrophysics Laboratory (LMSAL). The detector is a novel class of microcalorimeter, a superconducting Transition-Edge Sensor (TES), that coupled with associated SQUID and feedback electronics requires high temperature stability at ~100 mK to resolve the energy of absorbed X-ray photons emitted from the solar corona. The cooling system incorporates an existing Adiabatic Demagnetization Refrigerator (ADR) developed at the University of Wisconsin (UW), which was previously flown to study the diffuse cosmic X-ray background. [1,2] Modification of the UW ADR design, including TES focal plane and electronics re-positioning, therefore requires a tradeoff between the existing ADR solenoid nulling coil geometry and a low mass passive solenoid shield, while preserving the vibration isolation features of the existing design. The method of X-ray detection using microcalorimeters, including TES, is shown schematically in Figure 1.

The primary scientific goals of the ATTSI program are: 1) to demonstrate the performance of transition-edge sensors (TES) in microcalorimeter detectors for spaceborne spectro-heliograph instruments for solar physics observations, including future observatories; 2) to understand the use of high energy and imaging resolution in broad band observations; 3) to observe initial phase heating in the solar active regions using these detectors in a proof-of-concept sounding rocket demonstration, the Advanced Technology Solar Spectroscopic Imager (ATSSI) with an expected launch date in CY 2008; 4) to demonstrate the high sensitivity of TES to single photon events at low flux rates (X-rays from solar corona); and 5) to demonstrate enabling technologies such as cryostat design and adequate magnetic shielding of critical components. The primary engineering challenges are: 1) ADR cryostat modifications; 2) TES magnetic shielding requirements; 3) onboard controller/electronics; 4) data management (~ 120 Mb/sec/pixel rate); 5) acoustic & thermal loads; and 6) calibration, integration & testing.

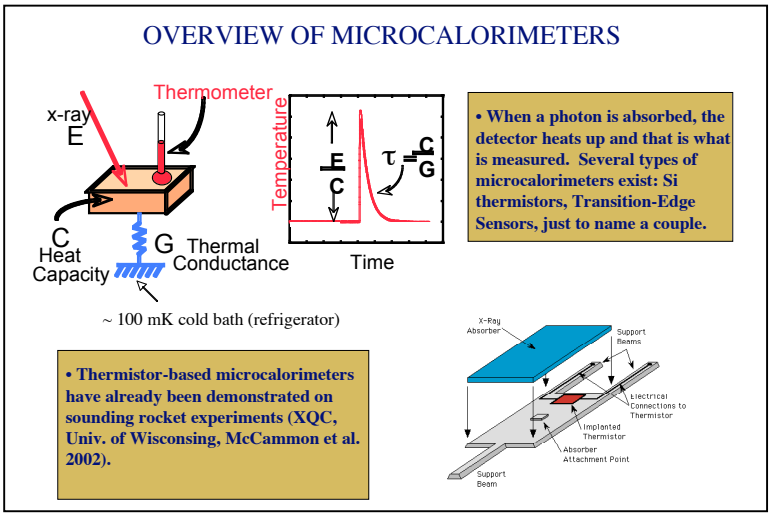

FIGURE 1. TES and Thermistor Microcalorimeter Detectors

ADR Design and Operation

An ADR comprises a strong superconducting solenoid, which has a high turn density to generate an intense axial central field, and a paramagnetic refrigerant capsule such as FAA suspended within the solenoid bore. Typically, the solenoid current is ramped slowly from zero to a safe maximum charging value to provide ~ 4T at the center of the solenoid and capsule. The axial induction component causes an alignment of the paramagnetic material's electron spins. During this isothermal magnetization phase the heat of magnetization is removed via a closed thermal switch to the near-surround heat sink, usually a superfluid helium bath at < 2 K. When the system is thermally equilibrated, the thermal switch is opened and the capsule and its detector heat load are thermally isolated. During the adiabatic demagnetization phase the solenoid current is reduced and the capsule cools in approximately direct proportion to the change in magnetic induction. In order to hold a constant final design temperature for long observation periods, the demagnetization is stopped before the field actually reaches zero. The current at this point is the initial operating current.

For the UW ADR solenoid the maximum charging current is 8.185 A and the initial operating current is 0.150 A, resulting in an initial net central field of ~0.0720 T. The current and field are gradually reduced as required to provide cooling to offset the thermistor detector dissipation and parasitic heat loads and to maintain a highly regulated detector temperature of ~ 100 mK. In the existing magnet design a secondary nulling coil is located just beyond the detector end of the main solenoid. The nulling coil carries ~ 95% of the main solenoid current, but in the opposite polarity, to generate a null condition (zero field on axis) at the detector focal plane, 3.9 cm from the main solenoid end. A second null point occurs just beyond the first, at about 4.7 cm. There is some adjustment provision for the null point locations by varying the nulling coil current. The nulling coil also provides a modest overall field magnitude reduction of ~ 20% at the FET housing location. One disadvantage of a single nulling coil design is that it provides at most two true null points. In the case of an ADR it also asymmetrically degrades the solenoid central field used to align the electron spins unless its current can be set to zero during the isothermal magnetization phase.

MODELS

Purpose of Model Development

We have developed two analytical models for analyzing the internally generated ADR magnetic fields to determine the acceptability of the existing cryostat design or the need for its modification for the TES application. In particular, the two models determine the net magnetic field induction of the UW ADR solenoid and / or nulling coil at arbitrary field points and for arbitrary currents. The models provide an assessment tool to determine the need to provide magnetic shielding at the detector focal plane or at critical electronics, such as SQUID amplifiers, or alternatively to fully or partially isolate the solenoid using a ferromagnetic shield. Because of the high vibration environment associated with sounding rocket experiments, any re-design or modification of the cryostat must have minimal impact on the optimized resonant characteristics of the as-designed system. Additionally, external fields associated with ADR operation in future space-borne payloads may cause interference with flight avionics or other experiments.

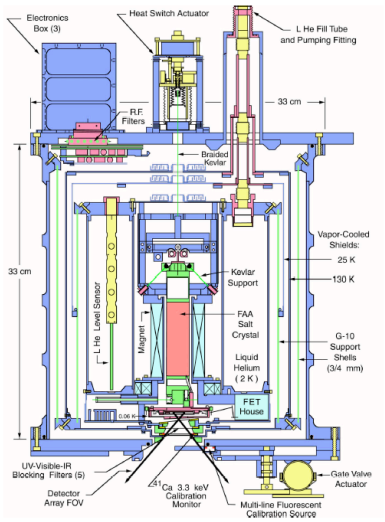

FIGURE 2. The University of Wisconsin ADR Cryostat and Thermistor Detector System

Model for Solenoid Shield Design

The design of a minimum mass soft ferromagnetic shield with given saturation induction Bsat to completely contain a given ADR solenoid central induction Bsol follows from the requirement that the axial magnetic flux be conserved across the vertical profile of the shield at either end of the magnet. Likewise the total flux at either end must be conserved in the cylindrical shell return just outside the solenoid. [3] These conditions can be obtained by integrating the solenoid induction over an arbitrary axi-symmetric circular area at the end of the solenoid. The existence of the iron (non-superconducting) shield itself ensures that the induction field within the fully shielded solenoid bore is highly uniform, unlike the unshielded short solenoid field itself, and has the same magnitude as the mid-plane induction. The proof follows from Gauss's Law, which can also be used to show that the induction falls off linearly in the radial direction across the winding thickness. The return flux is carried uniformly in the shield shell. It is convenient to divide the shield end profile into four regions (bore, windings, transition, and return) to carry out the integrations to determine the minimum shield thickness versus radius from the solenoid centerline. The uniform induction over the bore results in a linear increase in shield thickness from the bore center to the inside winding radius; the linear decrease in the induction across the windings results in a nonlinear height profile that exhibits a maximum as the vertical area*Bsat product initially increases faster with the radius than the end area*Bsol product. A nonlinear thickness roll-off continues over the transition until the profile drops to zero where it meets the edge of the cylindrical shell. Using well-known Bsat and density data for electromagnetic iron, 2V-permendur, or other soft iron material, the model determines the optimum profile and minimum mass of the shield to contain a maximum central induction. Previous measurements with a Hall probe positioned at the joint of a two-piece 4T solenoid shield with this design validated the design approach, with leakage onset at ~3.9 T as shown in Figure 3. To use the model, the solenoid geometry and maximum field current are entered in an EXCEL spreadsheet, the shield material is chosen, and the shield profile and mass are computed and charted. The UW ADR main solenoid current for a 4 T central field is 8.185 A and at 0.22 T the current is 0.45 A. The latter current value results in a shield mass of 0.26 kg, which is equal to the mass of the UW ADR nulling coil, but it still

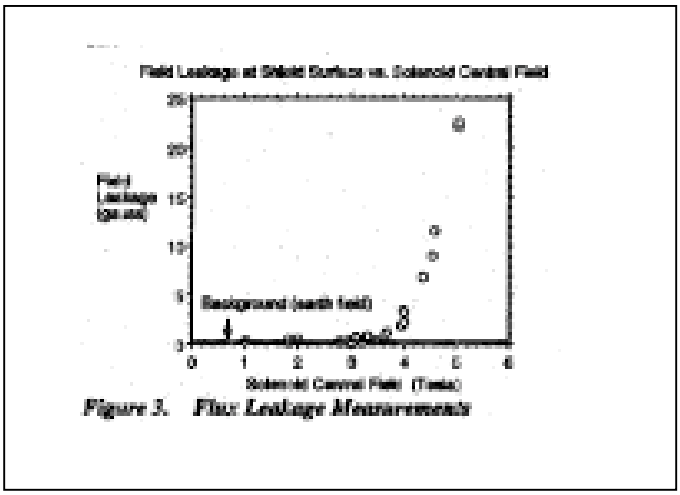

FIGURE 3. Experimental Leakage Data Using Shield Model Design for Shield Saturation at 4 Tesla

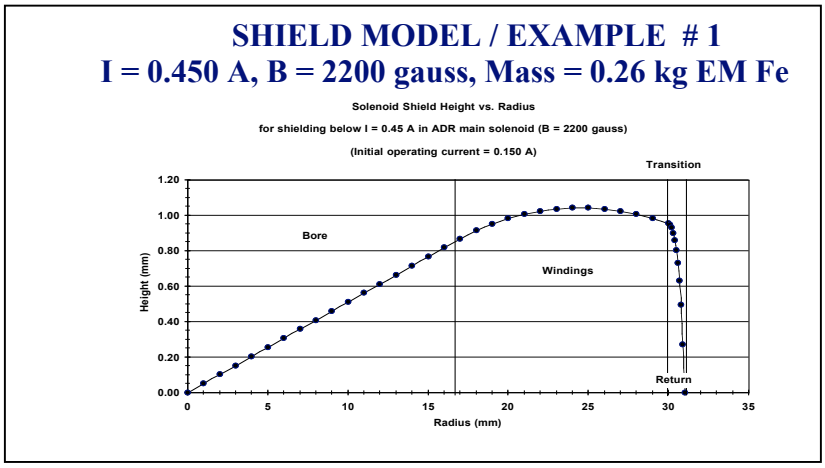

FIGURE 4. Shield Model Result for Equal Shield and Nulling Coil Masses

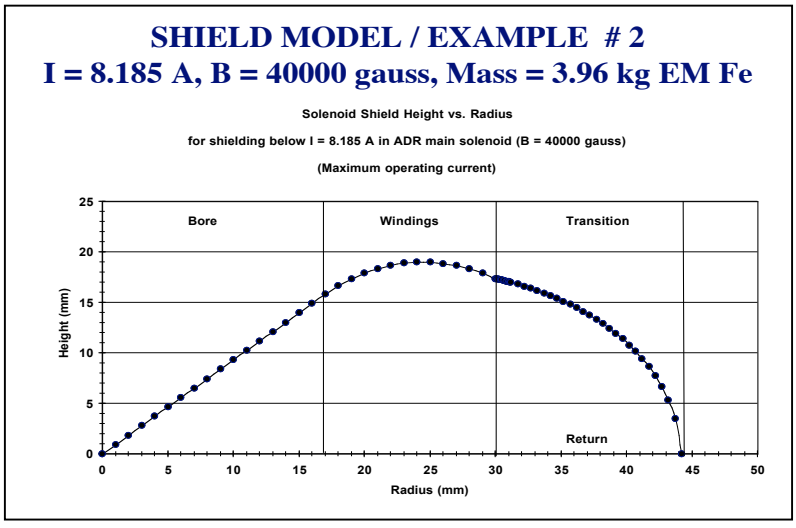

FIGURE 5. Shield Model Result for Maximum Current and Field

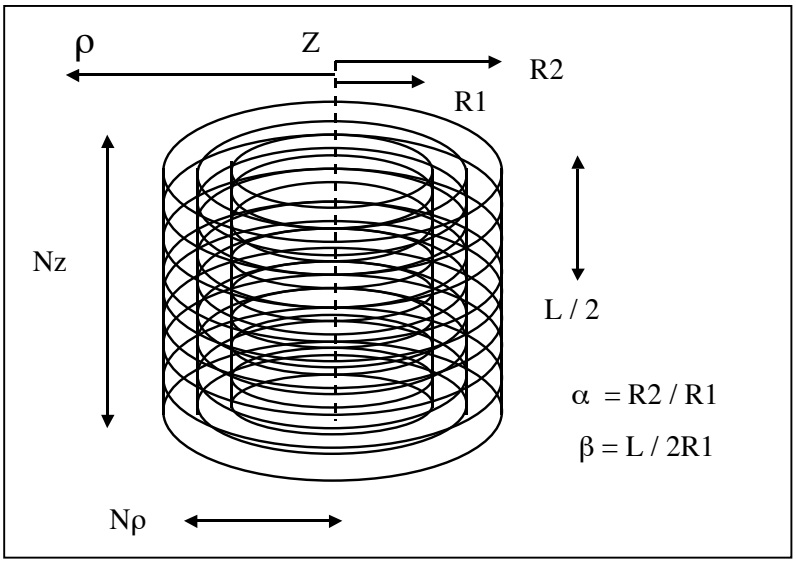

FIGURE 6. Model Schematic for Magnetic Induction Calculations at Arbitrary Field Points

provides full shielding at 3 times the initial operating current. The shield profile is shown in Figure 4. For comparison a shield for the full charging current requires a mass of 3.9 kg. Its profile is shown in Figure 5.

Model for Calculating Theoretical Magnetic Induction at an Arbitrary Field Point

An EXCEL spreadsheet model was devised for calculating the magnetic induction of an ADR solenoid and nulling coil system at an arbitrary field point (ρ, z) within or external to the magnet system. The model serves as an in-house resource to help make tradeoffs on the re-design of the ADR cryostat for the TES application. It can also supplement or confirm a solenoid manufacturer's field data or results of much more sophisticated models. [4] The model was developed in stages to ensure accuracy of the final version. It uses the principle of superposition of the fields of current loops (rings) to build up a system of concentric thin solenoids that can represent a thick solenoid. Because there is no simple analytical result for the field of a thick solenoid, this or similar approaches are widely discussed in the literature. [5-7] This method requires that the winding geometry, central field induction, and either the turn density or current of the modeled solenoid and nulling coil are given. A simplified schematic of the model is shown in Figure 6. Given the thick solenoid geometry and current, the turn density (~3.36 E7/m^2 for the UW solenoid) is derived from the known analytical formula for the central field. [8] The current is divided equally among the Nρ thin solenoids; all rings carry equal currents. The model calculates the fields of the thick solenoid and nulling coil independently as cylindrical induction field components Bz and Bρ and obtains magnitudes and angles with respect to the solenoid axis. Components are then added to obtain the net field components, and the net field magnitude and angle are computed.

The model development used well-known formulas for on-axis and near-axis fields for thin solenoids to identify any difficulties in the superposition method. [8] Two approaches were taken for the determination of the exact fields at an arbitrary point. The first method involved the derivation of the spherical coordinate induction components based on the magnetic scalar potential. [9-10] This requires expansions in the odd-numbered LeGendre

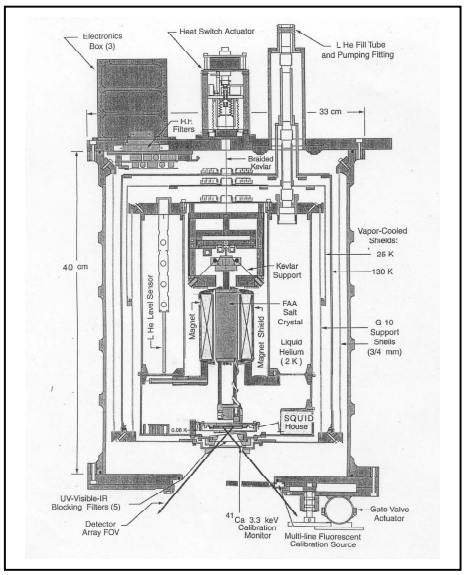

FIGURE 7. Proposed ADR Cryostat Modifications for TES Application

polynomials and their derivatives, and the spherical coordinate results are converted into the desired cylindrical components. Expansion terms for $r > R$ and $r < R$ are different, where r is the distance to the field point and R is the radius of a given ring. This approach proved to be ineffective for $r \sim R$, because convergence would have required terms much higher than P11, as used in the model. (Within and just beyond the solenoid there will always be a subset of rings for which $r \sim R$.) However, this method was retained for comparison to the results of the second approach for $r > 1.5$ R, where convergence of the polynomial expansion is rapid and the method is quite accurate. The second approach used the vector potential for a current ring to derive the induction components in either spherical or cylindrical coordinates. [6-7, 11] This approach provides closed form solutions (which can also be expanded), but here the problem is to accurately evaluate the complete elliptic integrals of the first and second kind. A method was found to do this analytically to within an accuracy of 2E-8. [12] Results of this method have been compared to limited published data (see Table 1). [7, 13] The radial and axial induction component contributions from a single ring of radius R are given in SI units [11] by:

$$B_\rho = (\mu_o I /2\pi) \{z /\rho [(R + \rho)^2 + z^2]^{1/2}\} \{-K + E (R^2 + \rho^2 + z^2) / [(R - \rho)^2 + z^2)]\} \quad (1)$$

$$B_Z = (\mu_o I /2\pi) \{z /\rho [(R + \rho)^2 + z^2]^{1/2}\} \{K + E (R^2 - \rho^2 - z^2) / [(R - \rho)^2 + z^2)]\} \quad (2)$$

K and E are the complete elliptic integrals of the first and second kind with modulus m

$$\text{where} \quad m = [1 - (1 - k^2)^{1/2}] / [1 + (1 - k^2)^{1/2}] \quad \text{and} \quad k^2 = 4R\rho / [(R + \rho)^2 + z^2)] \quad (3)$$

The model is user-friendly and flexible for the UW cryostat re-design trade-off. One proposed re-design is shown in Figure 7. In more general applications the solenoid and nulling coil geometries, central field values, and operating currents can be varied individually. One

TABLE 1. Comparison of Model Results to Published Data for a thick solenoid with $\alpha = 3$, $\beta = 2$ (D B Montgomery, Ref. 7). Field coordinates are measured from the axis at mid-plane.

ρ (R1)	0	0	0	2	2	2	5	5	5
z (R1)	0	1	2	0	1	2	0	1	2
Bz (DBM)	100.0	91.0	62.4	43.8	39.9	28.8	-4.6	-4.0	-2.4
Bz (Model)	100.00	91.05	62.46	44.13	40.90	28.95	-4.625	-4.015	-2.424
Bρ (DBM)	0	0	0	0	12.8	37.7	0	2.4	4.0
Bρ (Model)	0	0	0	0	12.69	41.00	0	2.59	4.18

problem for implementing the superposition method is to ensure that a sufficient number of vertical rings and concentric solenoids are used. The number of vertical rings can be varied from 2 to 200, but depending on the α and β values, $Nz = 50$ is usually adequate. It was found that model accuracy is significantly improved by using an averaging technique over the $N\rho$ concentric solenoid contributions. A curve-fit of order $N\rho - 1$ is integrated over the winding thickness. [13] The value of $N\rho$ in the current model is only seven, but it can be increased if necessary. The field point inputs (ρ, z) are referenced to the main solenoid and automatically re-referenced for the nulling coil calculations at the same point. To take into account the existence of a solenoid shield, the current at which the shield saturates is subtracted from the input current and the induction at any field point *external* to the shield is calculated. Solenoid shielding with superconducting materials has not yet been incorporated in the model. [14]

Preliminary Model Results and ADR Cryostat Re-design Options

Several cryostat re-design options have been identified by using the models: 1) retain the existing magnet and cryostat geometry; shield sensitive SQUID components as required based on model calculations for initial operating current, ~0.150 A; calculated fields range from 4 gauss to 23 gauss over the SQUID location; 2) as above, but relocate the TES detector from 3.9 cm to ~ 5.7 cm from end of solenoid (this requires 100% null current and location at the second null point); 3) provide an off-axis nulling coil at the SQUID location, using the model to design the nulling coil parameters; 4) relocate SQUIDs farther from the cryostat and use a thermal bus to ensure < 4 K; 5) eliminate the nulling coil and replace it with a ferromagnetic shield of equal mass (~ 0.26 kg), thereby eliminating all external field interference from the solenoid when its current is < 0.45 A, giving a safety factor of 3. A preliminary analysis of this option indicates that the magnet resonance characteristic would be unchanged; the detector could be relocated anywhere along the axis or off-axis, and the SQUID electronics could be re-positioned closer to the detector. However, potential degradation of the TES detector and SQUID electronics due to exposure to high fields during the charging cycle must be addressed. The re-designed cryostat based on this option is shown in Figure 7. The cryostat length has been extended from 33 cm to 40 cm to provide better accessibility to the focal plane and electronics, and thermal buses provide the 100 mK detector and 2 K SQUID cooling.

CONCLUSIONS

Two analytical models have been developed to guide the re-design options for the University of Wisconsin ADR cryostat for the TES detector application in ATTSI. They are both implemented as EXCEL spreadsheets with simple inputs. The field model provides accurate magnetic induction components due to the main thick solenoid and nulling coil system at any arbitrary field point as a tool for determining detector / electronics shielding requirements. It may also be used generally to define a new magnet system geometry. The shield model provides the minimum mass geometry of a soft iron shield to fully eliminate the induction at external field points for given solenoid operating parameters.

ACKNOWLEDGEMENTS

This work was supported in part by NASA Grant # NAG5-679.

REFERENCES

1. Cabrera, C. et al., "Cryogenic Detectors Based on Superconducting Transition Edge Sensors for Time-Energy Resolved Single-Photon Counters and for Dark Matteer Searches," in *Physica B* 46A, edited by U. B. Balachandran et al., Plenum, New York, 1999, pp. 651-654.
2. McCammon, D. et al., "A High Spectral Resolution Observation of the Soft X-Ray Diffuse Background with Thermal Detectors," in *The Astrophysics Journal* 576, 2002, pp. 188-203.
3. Corson, D. R. and Lorrain, P., *Introduction to Electromagnetic Fields and Waves*, W.H. Freeman and Company, San Francisco, 1962, pp. 295-297 and pp. 202-209.
4. For example, Poisson Superfish Code, Los Alamos National Laboratory, Superfish@lanl.gov
5. Nachamkin, J. and Maggiore, C. J., "A Fourier Bessel Transform Method for Efficiently Calculating the Magnetic Field of Solenoids," in *J. of Computational Physics.* 37, 1980, pp. 41-55
6. Jackson, J. D., *Classical Electrodynamics*, 2nd Edition, , John Wiley and Sons, Inc., New York, 1975, pp. 177-180.
7. Montgomery, D. B., *Solenoid Magnet Design*, Wiley-Interscience, New York, 1969, pp. 226-239.
8. Lorrain, P. and Corson, D.R., *Electromagnetic Fields and Waves,* W.H. Freeman and Company, San Francisco, 1970, pp. 325-326.
9. Page, L. and Adams, N. I., Jr., *Principles of Electricity*, *2nd Edition*, D. Van Norstrand Co., Inc., New York, 1949, pp. 254-257.
10. Jeans, Sir James, *The Mathematical Theory of Electricity and Magnetism,* 5th Edition, Cambridge, University Press, 1951, pp. 431-433.
11. Smythe, W. R., *Static and Dynamic Electricity*, 2nd Edition, McGraw-Hill Book Company, New York, 1950, pp. 274-275; 3rd Edition ,1968, pp. 290-291.
12. *Handbook of Mathemat ical Functions*, edited by M. Abramowitz and I. A. Segun, Dover Publications, New York, 1968, pp. 589-626.
13. Garrett, M. W., "Calculation of Fields, Forces, and Mutual Inductances of Current Systems by Elliptic Integrals," in *J. Appl. Phys.* 34, 1963, pp. 2567-2573.
14. Muething, K. A., et al., *Small Solenoid with a Superconducting Shield for Nuclear-Magnetic-Resonance near 1 Mk,* Rev. Sci. Instrum. 53 (4), 1982, p. 485.